DEUTSCHES ELEKTRONEN-SYNCHROTRON **DESY**

DESY 87-131
October 1987

SOME EXOTIC PHYSICS AT HERA

by

F. Cornet

Deutsches Elektronen-Synchrotron DESY, Hamburg

ISSN 0418-9833

NOTKESTRASSE 85 · 2 HAMBURG 52

To be sure that your preprints are promptly included in the HIGH ENERGY PHYSICS INDEX , send them to the following address (if possible by air mail) :

DESY
Bibliothek
Notkestrasse 85
2 Hamburg 52
Germany

DESY 87-131
October 1987

ISSN 0418-9833

Some Exotic Physics at HERA[1]

F. Cornet[2]

Deutsches Elektronen-Synchrotron DESY, Notkestrasse 85, D-2000 Hamburg 52, FRG

Abstract

We study possible signals of physiscs beyond the Standard Model that can be observed at HERA. In particular we concentrate on the effects of a second Z' taking the particular cases of E_6 Grand Unified theories and Left-Right Symmetric Models, and those of a possible four-fermion contact term derived from composite models.

[1] Invited lectures at XV International Winter Meeting on Fundamental Physics, Sevilla (Spain), Feb. 1987

[2] On leave from Departament de Física Teórica, Universitat Autonoma de Barcelona (Spain)

1. Introduction.

The Standard Model of the electromagnetic, weak and strong interactions is a extremely succesful theory from the experimental point of view. From the theoretical point of view, however, it still has some problems and shortcomings that led to the proposal of extensions or drastic modifications of the $SU(3)_C \times SU(2)_L \times U(1)_Y$ theory. The main problem stands in the Higgs sector, in particular, there is no mechanism to prevent the higgs mass to be of the order of the Planck scale, due to loop corrections to the bare mass. A rather unsatisfactory solution to this problem is to fine tune the bare mass in such a way that a cancelation with the loop contributions occurs leading to the desired mass $\leq 1\ TeV$. Two possibilities have been proposed to solve this problem:

1. Supersymmetry [1], where there is a cancelation between the contribution of the fermion loops and the one coming from the boson loops and
2. various types of composite models [2], where the higgs is assumed to be composite in such a way that the integrals in the loop calculations have to be cut-off at the compositeness scale, normaly of the order of $1TeV$. In these composite models one would expect also to be able to understand some questions that remain unanswered in the Standard Model, such as: the masses of the particles, or the number of generatios.

On the other hand, although the Standard Model unifies the electromagnetic and weak interactions, the strong interaction remains separated from the others. The Grand Unified Theories (GUT) [3] attempt to achieve this further unification assuming a gauge group G larger than $SU(3) \times SU(2) \times U(1)$ and such that contains the latter as a subgroup. Finally, attempts to include gravity led to the formulation of the superstring theories. These theories are, normally, formulated in a 10-dimensional space-time, but after the compactification process lead to a 4-dimensional, supesymmetric GUT.

The phenomenological predictions of all the theories and models that have been proposed are very similar to the Standard Model predictions at low energies, but deviations are expected to appear when going to higher energies. The search for these deviations will, then, be an important task of the new generation of accelerators. We cannot cover in these lectures all the possibilities that have been studied, rather we are going to study the modifications expected on the inclusive neutral current cross-sections in two different cases:

1. The presence of a new Z', taking as a reference some specific examples like E_6 GUT and Left-Right symmetric models.
2. The effects of a four-fermion contact interaction due, for instance, to some composite model.

Other cases, including the search for the supersymmetric partners of the ordinary particles and exotic colored particles, will be discussed by Buchmüller in his lectures [4].

2. Search for an Extra Neutral Gauge Boson.

2.1 Extra $U(1)$ from an E_6 Grand Unified Theory..

Since $SU(3) \times SU(2) \times U(1)$ is a subgroup of the GUT gauge group G, in any GUT the number of gauge bosons will be larger than in the Standard Model. In general, these new gauge bosons will be very massive, but in special cases some of them are predicted to have a mass of the order of the Fermi scale. We will study the expected signal of a second Z' for the extended electroweak gauge group: $SU(2)_L \times U(1) \times U(1)$ originated in the breaking of an E_6 GUT. The phenomenological studies of this new gauge boson started some time ago [5] and has recently received much attention due to superstring theories. It has been shown [6] that after the compactification process of the $E_8 \times E_8$ heterotic superstring on a non-compact Calabi-Yau manifold, one is left with a four dimensional E_6 GUT effective theory. Further breaking, through the wilson loop mechanism, of E_6 leads to the $SU(3) \times SU(2) \times U(1) \times U(1)$ group that can remain unbroken until low energies [7].

Since one can always rotate the neutral gauge sector in such a way that the first $U(1)$ in $SU(2)_L \times U(1) \times U(1)$ coincides with the normal weak hypercharge group, the modified lagrangian that describes the interaction of the neutral gauge bosons with fermions

$$L = eJ^{\mu}_{em}A_{\mu} + \frac{e}{\sin\theta_W \cos\theta_W} J^{\mu}_{NC} Z_{\mu} + g_{Y'} J'^{\mu} Z'_{\mu} \tag{1}$$

only differs from the usual neutral current lagrangian in the presence of the last term. Thus, A_μ is the photon field that couples to the electromagnetic current

$$J^{\mu}_{em} = \sum_f \bar{f}\gamma^{\mu} Q_f f, \tag{2}$$

where the sum extends over all the flavors f and Q_f is the corresponding electromagnetic charge, and Z_μ is the usual Z^0 field coupled to the current

$$J^{\mu}_{NC} = \sum_f \{\bar{f}_L \gamma^{\mu}(T_{3f} - \sin^2\theta_W Q_f) f_L + \bar{f}_R \gamma^{\mu}(-\sin^2\theta_W Q_f) f_R\}. \tag{3}$$

In (3) f_L and f_R denote the left and right handed components of the fermionic field and T_{3f} is the third component of the weak isospin. Finally, Z' in the third term of eq. (1) is the new neutral gauge boson field that couples to

$$J'^{\mu} = \sum_f (\bar{f}_L \gamma^{\mu} Y'_{f_L} f_L + \bar{f}_R \gamma^{\mu} Y'_{f_R} f_R), \tag{4}$$

where Y'_{f_L} and Y'_{f_R} are the charges to which the new Z' couples and depend on the model we study.

To fix the new charges Y'_{f_L} and Y'_{f_R} we assume that the extra $U(1)$ appears as the result of the breaking of the grand unification group E_6. The 15 fermions belonging to one generation, together with 12 new, exotic fermions are assigned to the fundamental representation of E_6. The particular values of the charges depend on the breaking scheme of this group into $SU(3)_C \times SU(2)_L \times U(1)_Y \times U(1)_{Y'}$. To parametrize the extra $U(1)$, consider the following scheme.

$$E_6 \to SO(10) \times U(1)_{\psi} \to SU(5) \times U(1)_{\chi} \times U(1)_{\psi}, \tag{5}$$

Table 1 Quantum numbers of the left-handed fields of a fermion 27-plet of E_6.

$SO(10)$	$SU(5)$	L-fields	$SU(3)_C$	Q	T_3	Y'
16	10	e^{-c}	1	1	0	$\frac{1}{2\sqrt{6}}\cos\alpha + \frac{1}{2\sqrt{10}}\sin\alpha$
		d	3	-1/3	-1/2	
		u	3	2/3	1/2	
		u^c	3^*	-2/3	0	
	5^*	d^c	3^*	1/3	0	$\frac{1}{2\sqrt{6}}\cos\alpha - \frac{3}{2\sqrt{10}}\sin\alpha$
		e^-	1	-1	-1/2	
		ν_e	1	0	1/2	
	1	$N_e{}^c$	1	0	0	$\frac{1}{2\sqrt{6}}\cos\alpha + \frac{5}{2\sqrt{10}}\sin\alpha$
10	5^*	h^c	3^*	1/3	0	$-\frac{1}{\sqrt{6}}\cos\alpha + \frac{1}{\sqrt{10}}\sin\alpha$
		E^-	1	-1	-1/2	
		ν_e	1	0	1/2	
	5	h	3	-1/3	0	$-\frac{1}{\sqrt{6}}\cos\alpha - \frac{1}{\sqrt{10}}\sin\alpha$
		E^{-c}	1	1	1/2	
		$N_E{}^c$	1	0	-1/2	
1	1	n	1	0	0	$\frac{2}{\sqrt{6}}\cos\alpha$

where the Standard Model group $SU(3)_C \times SU(2)_L \times U(1)_Y$ is a subgroup of $SU(5)$. The extra $U(1)$ will in general be a linear combination of $U(1)_\chi$ and $U(1)_\psi$ characterized by the angle α:

$$Z' = Z_{\psi}\cos\alpha + Z_{\chi}\sin\alpha. \tag{6}$$

Note that this is just a parametrization of the extra $U(1)$ and does not mean that E_6 must actually be broken following this scheme. A second comment is in order here. As can be seen in eq. (5) there are two additional $U(1)$ groups in E_6 originating two new, neutral gauge bosons: the one in eq. (6) and the orthonormal combination. We will introduce here the symplifying assumption that only Z' is light, while the orthonormal $U(1)$ is broken at a much higher scale and does not affect the low energy phenomenology. With these assumptions the charges for the left-handed fermions in the first generation are given in Table 1. Two identical copies of it describe the second and third generations.

The only parameter in the lagrangian, eq. (1), that remains to be fixed is the coupling constant $g_{Y'}$. We take for it the value

$$g_{Y'} = \sqrt{\frac{5}{3}}\frac{e}{\cos\theta_W}, \tag{7}$$

that comes from the assumption that the renormalization group evolution of $g_{Y'}$ is the same that the one of g_Y. The normalization of the coupling constant in eq. (7) and the charges in Table 1 are such that in the E_6 limit (when $\sin^2\theta_W = 3/8$) $g_{Y'}$ is equal to the $SU(2)_L$ coupling constant $g = e/\sin\theta_W$.

In general, the fields that will develop a mass in the symmetry breaking of $SU(2)_L \times U(1)_Y \times U(1)_{Y'}$ into $U(1)_{em}$ will not be Z and Z', but a mixture of these fields, Z_1 and Z_2,

given by

$$\begin{pmatrix} Z_1 \\ Z_2 \end{pmatrix} = \begin{pmatrix} \cos\theta & \sin\theta \\ -\sin\theta & \cos\theta \end{pmatrix} \begin{pmatrix} Z \\ Z' \end{pmatrix}, \tag{8}$$

where, without introducing new assumptions on the higgs sector, the angle θ can take any value in the range $-\pi/2 \leq \theta \leq \pi/2$. We will assign the low mass eigenstate, Z_1, to the observed particle. In the absence of mixing the Z_1 mass coincides with the Standard Model mass, m_Z, as can be seen in the relation

$$m_Z^2 = m_{Z_1}^2 \cos^2\theta + m_{Z_2}^2 \sin^2\theta \tag{9}$$

that can be deduced directely from eq. (8). This limit can also be approached for large values of m_{Z_2} since

$$tan^2\theta = \frac{m_Z^2 - m_{Z_1}^2}{m_{Z_2}^2 - m_Z^2} \tag{10}$$

vanishes when $m_{Z_2} \to \infty$.

The effective neutral current lagrangian written in terms of the mass eigenstates,

$$L = eJ_{em}^{\mu} A_{\mu} + \frac{e}{\sin\theta_W \cos\theta_W}(J_1^{\mu} Z_{1\mu} + J_2^{\mu} Z_{2\mu}), \tag{11}$$

where

$$\begin{aligned} J_1^{\mu} &= \cos\theta J_{NC}^{\mu} + \sin\theta \sqrt{\tfrac{5}{3}} \sin\theta_W J'^{\mu} \\ J_2^{\mu} &= -\sin\theta J_{NC}^{\mu} + \cos\theta \sqrt{\tfrac{5}{3}} \sin\theta_W J'^{\mu}, \end{aligned} \tag{12}$$

contains five free parameters. They are:

1. the angle α specifying the charges,
2. the two masses m_{Z_1} and m_{Z_2},
3. the mass mixing angle θ and
4. the Weinberg angle $\sin^2\theta_W$.

To further reduce the number of free parameters, we can assume that the higgses responsible of the electroweak symmetry breaking are all in doublets or singlets of $SU(2)_L$, as it is suggested in superstring theories. In this case, we have an additional relation,

$$\rho = \frac{m_W^2}{m_Z^2 \cos\theta_W} = 1, \tag{13}$$

that allows us to write $\sin^2\theta_W$ in terms of the two physical masses and the mass mixing angle

$$\sin^2\theta_W = \frac{1}{2}\left(1 - \sqrt{1 - \frac{4\mu^2}{m_Z^2}}\right), \tag{14}$$

where m_Z depends on m_{Z_1}, m_{Z_2} and θ as it is expressed in eq. (9), and

$$\mu^2 = \frac{\pi\alpha(m_e)}{\sqrt{2}G_F(1 - \Delta r)} = 38.65\ GeV \tag{15}$$

includes the Standard Model one loop radiative corrections, $\Delta r = 0.070 \pm 0.002$ [9]. In our numerical calculations we will take $m_{Z_1} = 93.3\ GeV$ and then calculate $\sin^2\theta_W$ according to the preceding formulae as a function of m_{Z_2} and θ.

We are now in position to calculate the cross-sections of deep inelastic $e^-_{L,R}p$ scattering. In terms of the usual variables $Q^2 = -q^2$ and $x = -q^2/2pq$, where q is the four-momentum of the exchanged boson and p is the one of the incoming proton, it is given by [10]

$$\frac{d\sigma(e^-{}_{L,R})}{dxdQ^2} = \frac{2\pi\alpha^2}{xQ^4}(1 + (1-y)^2)\left(F_2^{L,R}(x,Q^2) + h(y)xF_3^{L,R}(x,Q^2)\right), \tag{16}$$

where $y = Q^2/xs$ ($\sqrt{s}$ is, as usual, the center of mass energy that for our numerical examples we will take to be the maximum HERA energy $\sqrt{s} = 314\ GeV$) and $h(y) = \{1-(1-y)^2\}/\{1+(1-y)^2\}$. The functions

$$\begin{aligned} F_2^{L,R}(x,Q^2) &= \textstyle\sum_f \{xq_f(x,Q^2) + x\bar{q}_f(x,Q^2)\}\tilde{F}_{2_f}^{L,R}(Q^2), \\ xF_3^{L,R}(x,Q^2) &= \textstyle\sum_f \{xq_f(x,Q^2) - x\bar{q}_f(x,Q^2)\}\tilde{F}_{3_f}^{L,R}(Q^2) \end{aligned} \tag{17}$$

contain the scaling violating quark and antiquark distribution functions in the proton, $q_f(x,Q^2)$ and $\bar{q}_f(x,Q^2)$, and the electroweak charges and parameters that enter in

$$\begin{aligned} \tilde{F}_{2_f}^{L,R}(Q^2) &= Q_f^2 + \textstyle\sum_{i=1}^2 \{(v_{ie} \pm a_{ie})^2(v_{if}{}^2 + a_{if}{}^2)P_i{}^2 - 2Q_f(v_{ie} \pm a_{ie})v_{if}P_i\} \\ &\quad +2(v_{1e} \pm a_{1e})(v_{2e} \pm a_{2e})(v_{1f}v_{2f} + a_{1f}a_{2f})P_1P_2, \end{aligned} \tag{18}$$

$$\begin{aligned} \tilde{F}_{3_f}^{L,R}(Q^2) &= \pm 2\{\textstyle\sum_{i=1}^2 \left((v_{ie} \pm a_{ie})^2 v_{if}a_{if}P_i{}^2 - Q_f(v_{ie} \pm a_{ie})a_{if}P_i\right) \\ &\quad +(v_{1e} \pm a_{1e})(v_{2e} \pm a_{2e})(v_{1f}a_{2f} + a_{1f}v_{2f})P_1P_2\}, \end{aligned}$$

where $P_i = Q^2/(Q^2 + m_{Z_i}{}^2)$ are essentially the Z_i propagators and v_{i_f} and a_{i_f} are the vector and axial charges that, taking into account the $Z - Z'$ mixing, take the form

$$\begin{aligned} \begin{pmatrix} v_{1_f} \\ v_{2_f} \end{pmatrix} &= \tfrac{1}{\sin 2\theta_W} \begin{pmatrix} \cos\theta & \sin\theta \\ -\sin\theta & \cos\theta \end{pmatrix} \begin{pmatrix} T_{3_f} - 2Q_f \sin^2\theta_W \\ \sqrt{\frac{5}{3}}\sin\theta_W(Y'_{f_L} + Y'_{f_R}) \end{pmatrix} \\ \begin{pmatrix} a_{1_f} \\ a_{2_f} \end{pmatrix} &= \tfrac{1}{\sin 2\theta_W} \begin{pmatrix} \cos\theta & \sin\theta \\ -\sin\theta & \cos\theta \end{pmatrix} \begin{pmatrix} T_{3_f} \\ \sqrt{\frac{5}{3}}\sin\theta_W(Y'_{f_L} - Y'_{f_R}) \end{pmatrix}. \end{aligned} \tag{19}$$

The positron cross-sections $d\sigma(e^+_{L,R})/dxdQ^2$ can be obtained from eq. (16) replacing $F_2^{L,R} \to F_2^{R,L}$ and $xF_3^{L,R} \to -xF_3^{R,L}$. When taking the limit $m_{Z_2} \to \infty$, that is $P_2 \to 0$ and $\theta = 0$ we recover the Standard Model expressions [11]. The cross-sections, however, are not the most sensitive quantities to look for the presence of the second Z. We will also be interested in studying the deviation from the Standard Model predictions for the six asymmetries that can be constructed if polarized electron and positron beams are available:

1. two polarization asymmetries

$$A^{\pm\pm}_{LR} = \frac{d\sigma^{\pm}_{L} - d\sigma^{\pm}_{R}}{d\sigma^{\pm}_{L} + d\sigma^{\pm}_{R}}, \tag{20}$$

2. two charge asymmetries

$$A^{-+}_{\substack{LL\\RR}} = \frac{d\sigma^{-}_{\substack{L\\R}} - d\sigma^{+}_{\substack{L\\R}}}{d\sigma^{-}_{\substack{L\\R}} + d\sigma^{+}_{\substack{L\\R}}}, \tag{21}$$

3. and two mixed asymmetries

$$A^{-+}_{\substack{LR\\RL}} = \frac{d\sigma^{-}_{\substack{L\\R}} - d\sigma^{+}_{\substack{R\\L}}}{d\sigma^{-}_{\substack{L\\R}} + d\sigma^{+}_{\substack{R\\L}}}. \tag{22}$$

Note that since there are only four independent structure functions, eq. (17), only four of these asymmetries are independent. We will study, however, all of them because we do not know a priori which one is more sensitive to the Z' presence.

We first want to identify what are the charges for which the effects of the second Z are larger. So, in Fig.1 we plot the six asymmetries as a function of $\cos\alpha$ [18] [3]. In these plots we fix the other free parameters to be: $m_{Z_2} = 200\ GeV, \theta = 0$. We have chosen the kinematical point $x = 0.3$ and $Q^2 = 20000\ GeV^2$, which gives a rather accurate idea of the effects one can expect to see in a more realistic situation as will be shown later. The dotted lines are the Standard Model predictions for each asymmetry. Since we have chosen a particular kinematical point, this is just a number and appears as a horizontal line in the plots. We already observe that the effects of the presence of Z_2 will be very different in different asymmetries in such a way that we will have to look for the most sensitive asymmetry in each model we study. This will never be A^{-+}_{LL} which, although has very large values, turns out to show very small deviations in the whole range of $\cos\alpha$. In any case, for $\cos\alpha \leq -0.5$ the difference between the Standard Model and the two Z model predictions, $\delta A = |A(Z_1, Z_2) - A(Z)|$, is very small for all the asymmetries ($\delta A \leq 0.03$), thus making the search for for Z_2 in these models very difficult. We can also observe in Fig. 1 that for almost all the asymmetries, except for A^{++}_{LR}, there are two values of $\cos\alpha$ for which $\delta A = 0$. Almost all of them depend on the kinematical point we have chosen to plot these curves. The two exceptions are $\cos\alpha = 3\sqrt{6}/8$ in A^{-+}_{LR} and $\cos\alpha = -\sqrt{6}/4$ in A^{-+}_{RL}. These mixed asymmetries turn out to be proportional to the left and right handed couplings of the electron to Z_2, respectively, and those values of α are such that $L_{e_2}(\cos\alpha = 3\sqrt{6}/8) = 0$ and $R_{e_2}(\cos\alpha = -\sqrt{6}/4) = 0$. These zeroes, however, will move when changing the value of θ because of the contribution from L_e and R_e that enters into L_{e_2} and R_{e_2} through the mixing mechanism (see eq. (19)). Some bounds on m_{Z_2} have already been obtained from the available experimental data [12,13,14]. Imposing that the agreement between the experimentally measured $|V_{ud}|^2 + |V_{us}|^2 + |V_{ub}|^2 = 0.9984 \pm 0.0021$ and the unitarity value of 1 is not spoiled by the contribution of Z_2 trhough

[3] In all our numerical calculations we use the quark distribution functions of Duke and Owens (set I) [19].

the box diagrams of Fig. 2, Marciano and Sirlin [12] have shown that $m_{Z_2} \leq 200\ GeV$ is already excluded in the range $-0.7 \leq \cos\alpha \leq 0.4$. The strongest bound, $m_{Z_2} \leq 275\ GeV$, is obtained for $\cos\alpha \simeq -0.26$, while in the range $\cos\alpha \geq 0.67$ and $\cos\alpha \leq -0.91$ no interesting bound (lower than $100 GeV$) is found with this method.

Among all the models shown in Fig. 1 there are three theoretically preferred possibilities for Z'. Model A is defined by $\cos\alpha = \sqrt{5/8}$ and appears in the no-scale supergravity scenario [15], where E_6 is broken at the compactification scale down to $SU(3)_C \times SU(2)_L \times U(1)_Y \times U(1)_{Y'}$ which remains unbroken until the Fermi scale. In models B and C one starts with two extra $U(1)$ and one of them is broken via large vacuum expectation values of the $SU(3)_C \times SU(2)_L \times U(1)_Y$ singlets n and N^c_e respectively. Model B is then characterized by $\cos\alpha = 0$ and model C by $\cos\alpha = -\sqrt{15/16}$. These two last models have the attractive feature that can accomodate light neutrinos in a natural way [16,17]. We choose these models for a more detailed analysis of the dependence of the effects due to the Z_2 on the mass m_{Z_2} and mixing angle θ. We show in Fig. 3 the contours for $\delta A = 0.04$ in the plane (θ, m_{Z_2}) for the three models and for the most sensitive of the polarization (solid line), charge (dash-dotted line) and mixed (dashed line) asymmetries in each case [18]. Preliminary analises show that this precission can be achieved with a careful study of the Q^2 dependence (see [11] for a similar study of the sensitivity of the asymmetries on $\sin^2\theta_W$). The kinematical point used here is the same as in Fig. 1, namely $x = 0.3$ and $Q^2 = 20000\ GeV^2$. The present experimental bounds from an analysis of all the available neutral current data, including ν-hadron, νe, eN, μN, e^+e^- and direct production in the $Sp\bar{p}S$ collider [13] for models A and B are also included (thick line) and have been extrapolated to larger values of m_{Z_2} following their asymptotic behaviour of $1/m_{Z_2}$ (dotted line). If no effect with $\delta A \geq 0.04$ is observed, the mass m_{Z_2} and mixing angle θ are restricted to the interior of the curves (region of large mass and small mixing angle).

Two regions can be distiguished in these plots. The region of lower m_{Z_2} and small mixing angle, and the region of large m_{Z_2}. In the latter region one is probing the dependence of the asymmetries on $\sin^2\theta_W$, while the contribution of the terms including the exchange of Z_2 is very small. For this reason, the contours are very similar in all models in this region and the most sensitive asymmetry is $A^{-+}_{L\bar{R}}$ (see ref. [20]), while the mixed asymmetry $A^{-+}_{R\bar{L}}$ essentially provides no bounds. More interesting for us is the first region where the effects of the Z_2 propagator manifest. The contours are now much more model dependent and open the possibility of discriminating among different models if an effect is observed. As was expected from Fig. 1 the effects induced by model C are rather small and it will be very difficult to probe masses larger than $\sim 150\ GeV$. Model B is slightly more sensitive and masses up to $\sim 200\ GeV$ could be observed. Finally, in model A the mixed asymmetry $A^{-+}_{R\bar{L}}$ allows to probe masses up to $\sim 300 - 350\ GeV$ well above the present bounds [13].

To finish this section I will briefly summarize the expected effects of Z_2 in other future colliders. In e^+e^- collisions at the Z_1 peak direct effects produced by the Z_2 propagator will be hidden in the huge background. A precise measurement of Z_1 properties will, however, allow to get strong constrains in the value of θ. For example, comparing the values of the Weinberg angle obtained from measurements of the W and Z_1 masses,

$$\sin^2\bar{\theta}_W = 1 - \frac{{m_W}^2}{{m_{Z_1}}^2}, \tag{23}$$

and from the couplinbg constants,

$$\sin^2\theta_W = \frac{{g_Y}^2}{g^2 + {g_Y}^2}, \tag{24}$$

we can deduce a model independent bound for the mixing angle. The Standard Model predicts $\Delta = \sin^2\tilde{\theta}_W - \sin^2\theta_W = 0$, but in the two Z model the mixing mechanism induces a non-zero value for Δ. In this way a bound $\Delta \leq 0.002$ implies $|\theta| \leq 1^o$ for $m_{Z_2} \geq 100\ GeV$. In model A a better bound $|\theta| \leq 0.5^o$ can be obtained using the polarization asymmetry defined by

$$A_{POL} = \frac{\sigma_R - \sigma_L}{\sigma_R + \sigma_L}, \tag{25}$$

where σ_R and σ_L are the total cross-sections for right and left handed incident electrons (the positron beam is kept unpolarized) [21]. The required luminosity to achieve this precission is $L = 100\ pb^{-1}$. To study the case $\theta = 0$ in an interesting mass range one has to go to energies higher than those of LEP 1 or SLC [21,22]. If $m_{Z_2} \leq 190\ GeV$ very clear peaks in the cross-sections can be observed. The shape of the peak depends on the masses of the exotic fermions appearing in the fundamental representation of E_6. In the case that direct production is not kinematically allowed, effects of Z_2 can still be observed in the asymmetries. The most sensitive asymmetry for models A and C is A_{POL} defined in eq. (25), while the forward-backward asymmetry is the most suitable one to study model B [22]. As an example we show in Fig. 4 the polarization asymmetry, calculated using the expressions in Ref.[22], for the three models with $m_{Z_2} = 250\ GeV$ and $\theta = 0$ and compare them to the Standard Model prediction. We have taken $\Gamma_{Z_2} = 27 m_{Z_2}/1000$ which is common to all the models and corresponds to the case where all the decays into pairs of exotic fermions and all the supersymmetric partners are kinematically allowed (see Table 2). The conclusions do not change if we take the other extreme assumption, namely that Z_2 can only decay into known fermions. In this case, though, Γ_{Z_2} depends on the model. As can be observed there are appreciable differences with the Standard Model predictions at as a low an energy as 160 GeV (in model A, for instance, $\delta A_{POL}/A_{POL} \sim 20\%$).

The most efficient way of observing a new Z in proton-(anti)proton collisions is through its decay into electron or muon pairs. This has been, indeed, the way in which the Z has been discovered at CERN collider [23]. One has to reconstruct the Z_2 resonance produced via $q\bar{q}$ annihilation from the observed lepton pair. The cross-section and, consequently, the detection limits depend on the branching ratio $BR(Z_2 \to e^+e^-, \mu^+\mu^-)$ and the total width Γ_{Z_2}. We are going to consider here the two extreme cases: i) Z_2 is kinematically allowed to decay only into the known fermions (including the top quark as 'known') and ii) There is no kinematical suppresion for Z_2 to decay into exotic fermions and all the supersymmetric partners. In Table 2 we list the total width Γ_{Z_2} and branching ratio $BR(Z_2 \to e^+e^-)$ for the three models we are considering and cases i) and ii) [24]. Here and up to the end of this section we take $\theta = 0$.

With these quantities fixed one can calculate the cross-section $\sigma(p\bar{p} \to e^+e^-X)$ as a fuction of m_{Z_2} and estimate the detection limits in the three models we are considering. These are shown in Table 3 for the four present and future hadron colliders [24]: $Sp\bar{p}S$ (including ACOL) with a total center of mass energy $\sqrt{s} = 630\ GeV$ and a luminosity

Table 2. Z_2 total width and branching ratio into e^+e^- for cases i (and ii) [24]

model	Γ_{Z_2} (in units $m_{Z_2}/1000$)	$BR(Z_2 \to e^+e^-)$
A	4.5(27)	3.6(0.6)
B	8.2(27)	5.9(1.8)
C	4.5(27)	5.4(0.9)

Table 3. Detection limits in hadron colliders. The masses are in GeV[24]

model	$S\bar{p}pS$	Tevatron	LHC	SSC
A	110(160) [13]	170(280) [26]	2200(3100)	3400(5200) [27]
B	130(170)	230(310)	2700(3300)	4500(5700)
C	100(160)	160(270)	2200(3100)	3500(5200)

$L = 10^{30}\ cm^{-2}s^{-1}$, $p\bar{p}$ collisions at Tevatron with $\sqrt{s} = 2\ TeV$ and $L = 10^{30} cm^{-2}s^{-1}$ and pp collisions at $\sqrt{s} = 17\ TeV$ (LHC) and 40 TeV (SSC) both with $L = 10^{33} cm^{-2}s^{-1}$. We have requiered for the detection limit a total of 10 events per year of 10^7 seconds. Such high values for the masses, however, do not allow to investigate what are the couplings of Z_2 to the fermions and distinguish between different models. For that purpose one has to study the forward-backguard asymmetry [24,27,28] and more than 10 events are clearly requiered.

2.2 *Left-Right Symmetric Models.*

The original motivation to consider Left-Right symmetric models is the attempt to understand the origin of parity violation and introduce it through espontaneous symmetry breaking process as a non-invariance of the vacuum. A by product advantage is that they also allow to understand the smallnes of the cp symmetry breaking [8]. The simplest of the Left-Right models is based in the group $SU(3)_L \times SU(3)_R \times U(1)_{B-L}$ and, due to the existence of a discrete parity symmetry, $g_L = g_R$ before the symmetry breaking. The fermion quantum numbers are

$$\begin{array}{ll} l_L = (1/2, 0, -1) & l_R = (0, 1/2, -1) \\ Q_L = (1/2, 0, 1/3) & Q_R = (0, 1/2, 1/3), \end{array} \tag{26}$$

where the $U(1)$ generator corresponds to the difference between the baryon (B) and lepton (L) quantum numbers. The electric charge is then given by $Q = T_{3L} + T_{3R} + (B - L)/2$. Notice that a right-handed neutrino naturally appears in these theories allowing for a natural explanation of the smallness of the neutrino mass [29].

The neutral current current lagrangian

$$L = g_L W^\mu_{3L} J_{3L_\mu} + g_R W^\mu_{3R} J_{3R_\mu} + \frac{1}{2} g_C C^\mu J_{B-L_\mu} \tag{27}$$

describes the interaction of the gauge bosons W_{3L}, W_{3R} and C associated with the neutral generators T_{3L}, T_{3R} and $B - L$, respectively, with the fermions. In eq. (27) we have kept

$g_R \neq g_L$ because the discrete symmetry that keeps both coupling constats equal to each other might be broken at a higher scale than the gauge group. This question depends on the choice of the higgs structure one makes and here, as we did in the previous section, our only assumption on the higgs sector is that the higgses appear only in doublets and/or singlets of $SU(2)_L$ in such a way that the relation $\rho = 1$ still holds. The neutral gauge bosons W_{3L}, W_{3R} and C can be rotated to a basis containing the photon, A, the normal Z and the new gauge boson Z' through the transformation

$$\begin{aligned} W_{3L} &= x_L^{1/2} A + (1-x_L)^{1/2} Z \\ W_{3R} &= x_R^{1/2} A - (x_L x_R)^{1/2}(1-x_L)^{-1/2} Z + (1-x_L-x_R)^{1/2}(1-x_L)^{-1/2} Z' \\ C &= (1-x_L-x_R)^{1/2} A - (1-x_L-x_R)^{1/2} x_L^{1/2}(1-x_L)^{-1/2} Z - x_R^{1/2}(1-x_L)^{-1/2} Z', \end{aligned} \tag{28}$$

where $x_L = e^2/g_L^2$ can be identified with $\sin^2\theta_W$, $x_R = e^2/g_R^2$ is the equivalent quantity in the right-handed sector and the electric charge is given by $e^{-2} = g_L^{-2} + g_R^{-2} + g_C^{-2}$. In this way we can rewrite the lagrangian (27) in the form

$$L = e J^\mu_{em} A_\mu + \frac{e}{x_L^{1/2}(1-x_L)^{1/2}} J^\mu_{NC} Z_\mu + \frac{e}{x_R^{1/2}(1-x_L)^{1/2}(1-x_L-x_R)^{1/2}} J'^\mu Z'_\mu, \tag{29}$$

which has the same structure as eq. (1). The currents J^μ_{em} and J^μ_{NC} are given by eq. (2) and (3) respectively and

$$J'^\mu = x_R J^\mu_{3L} + (1-x_L) J^\mu_{3R} - x_R J^\mu_{em} \tag{30}$$

with

$$\begin{aligned} J^\mu_L &= \textstyle\sum_f \overline{f} \gamma^\mu T_{3Lf} f, \\ J^\mu_R &= \textstyle\sum_f \overline{f} \gamma^\mu T_{3Rf} f, \end{aligned} \tag{31}$$

From this point on the analysis of the effects induced by the new gauge boson follows the steps of the previous section. The free parameters we have now are

1. m_{Z_1}, the lowest mass eigenstate that we fix to be 93.3 GeV,
2. m_{Z_2}, the highest mass eigenstate,
3. θ, the mass mixing angle and
4. x_R, that is equivalent to the right-handed coupling constant.

Notice that x_L has been already excluded from the list of free parameters since we have fixed $\rho = 1$, which allows us to calculate x_L in terms of m_{Z_1}, m_{Z_2} and θ (see section 2.1).

In our numerical analysis of the effects of the new, neutral gauge boson we take as an example $x_L = x_R$. Indeed, we have already studied one case with $x_L \neq x_R$. Model B in the previous sectioncan be obtained as the result of the breaking of $SU(2)_R$ into a right-handed $U(1)$ at a scale higher than the Fermi scale. The only difference is an overall sign in our previous definition of the charges in modelB. This, however, has no physical significance and only manifests as a change in the definition of the mixing angle θ ($\theta \to -\theta$). The value of

x_R corresponding to this case is given by $x_R = 3(1-x_L)/5$. In Fig. 5 we show the contour plots for $\delta A = 0.04$ in the case $x_R = x_L$ for the most sensitive of the polarization (solid line), charge (dash-dotted line) and mixed (dashed line) asymmetries. The present experimental bounds taken from Ref. [13] are also shown (thick line) with the extrapolation to larger values of m_{Z_2} following the behaviour $1/m_{Z_2}$ (dotted line). The kinematiocal point chosen for this plot is, again, $x = 0.3$ and $Q^2 = 2 \times 10^4\ Gev^2$ in such a way that these curves can be directely compared to the ones in Fig. 3. The Z_2 masses for $\theta = 0$ that can be reached in this case are much higher ($m_{Z_2} \simeq 600\ GeV$) than the ones obtained in Sect. 2.1. This shows the sensitivity of the bounds at zero mixing angle to the charges to which Z' couples and, in particular when comparing to model B, to the coupling constant.

3. Contact Terms.

During the last years it has been speculated wether the quarks and leptons are elementary or have themselves a substructure. Although there is no fully consistent composite model, it is interesting to experimentally look for signals of the compositness. One has then to look for rather general effects that should be shared by all the realistic models one could think of. These effects can be clasified in two groups. First of all, one expects to have new particles, like excited states of quarks and leptons or even exotic states (leptoquarks, leptogluons,....). The search for these new particles is dicussed by Büchmuller in his lectures [4]. Second, The interactions between the fermions should show some departure from the Standard Model predictions when going to an energy high enough to probe the substructure. We are going to concentrate in this second case.

The radius of the quarks and leptons is characterized by the energy scale Λ through $R = O(1/\Lambda)$. Of course, this is not a very precise definition because Λ depends on the process used to probe it. In deep inelastic scattering the principal sensitivity is to Λ_{eq}. At momentum transfer of the order of Λ the interaction is dominated by hard processes among the constituents, while at low Q^2 the Standard Model is a good approximation for the effective interaction. At intermediate energies some residual interactions should manifest. These residual interactions are normally described by higher dimension operators scaled by powers of $1/\Lambda$ [30]. Of course, we only have to consider the lowest dimension operator involving four fermions because the other terms will be suppresed by powers of $\sqrt{s}/\Lambda$.

The effective lagrangian that we are going to consider [30,31],

$$L_{EFF} = L_{SM} + \epsilon \frac{g^2}{\Lambda^2} \sum_{a,b,f} C^f_{a,b} (\overline{e}_a \gamma^\mu e_a)(\overline{q}_{f_b} \gamma_\mu q_{f_b}), \tag{32}$$

contains the Standard Model lagrangian, L_{SM}, corrected by an electron-quark four fermion contact term that conserves helicity (the helicity violating terms are expected to be suppresed by powers of m_e/Λ). In eq. (32) the sum extends over the left and right components, a and b, of the fermionic fields and over all the quark flavors f. ϵ can take the values ± 1 and indicates wether the new contribution adds or subtracts from the Standard Model lagrangian. Finally,

the coupling constant g is supposed to be large. We take $g^2/4\pi = 1$, which is, indeed, a definition of Λ. The constants $C^f_{a,b}$ determine what is the helicity structure of the contact interaction for each quark flavor. To get an idea of what is the role played by the different structures we will study the following cases separately:

1. LL - $C_{LL} = 1$ and $C_{LR} = C_{RL} = C_{RR} = 0$,
2. LR - $C_{LR} = 1$ and $C_{LL} = C_{RL} = C_{RR} = 0$,
3. RL - $C_{RL} = 1$ and $C_{LL} = C_{LR} = C_{RR} = 0$,
4. RR - $C_{RR} = 1$ and $C_{LL} = C_{LR} = C_{RL} = 0$,
5. VV - $C_{LL} = C_{LR} = C_{RL} = C_{RR} = 1$,
6. AA - $C_{LL} = C_{LR} = C_{RL} = C_{RR} = -1$,

where the first letter refers to the electron and the second to the quark helicity structure that enter in the contact interaction. In our numerical examples we take the favorable case $\epsilon = 1$. The analysis for $\epsilon = -1$ is similar to the one shown here (although slightly more involved due to destructive interference effects) and leads to detection limits for Λ which are normally 1 or 2 TeV below the ones obtained for $\epsilon = +1$ [32].

The cross-sections for scattering of polarized electrons on protons can be easilly obtained from eqs. (16), (17) and (18) introducing $P_z = \alpha Q^2/\Lambda^2$ and the appropriate charges for each model. In Fig. 6 we plot

$$F(x,Q^2) = \frac{\frac{d\sigma}{dxdy}}{\frac{2\pi\alpha^2(1+(1-y)^2)}{sx^2y^2}} \tag{33}$$

as a function of Q^2 with $x = 0.3$ for the six models we are considering with $\epsilon = +1$ and$\Lambda = 3\ TeV$ and for the four possible electron polarizations. Significant deviations from the Standard Model predictions (dotted line) begin to appear at $Q^2 \sim 5000\ GeV^2$ for all the models, except for the RL and RR models in e^-_L and e^+_R cross-sections and for the LL and LR models in e^-_R and e^+_L cross-sections because these cases are not sensitive to the contact term. The use of polarized beams allows to determine the helicity structure of the new interaction. We can see in Fig. 6 that a VV contact term gives large effects in the four cross-sections, while the AA case induces appreciable deviations from the Standard Model in all the cross-sections except in e^+_R. The LL model can be distinguished from the LR because the former only gives large effects for the e^-_L cross-section and the second for the e^+_R one. Finally, something similar happens for the RL and RR models, where the deviations from the Standard Model predictions appear in the e^+_L and e^-_R respectively.

Similar comments to the ones in the preceding paragraph apply to the asymmetries, which also allow for the differentiation among the models. We show in Fig. 7a the values of the A^{--}_{LR} asymmetry for the LL and RR models as a fuction of Q^2 and for different values of Λ. This is the most sensitive asymmetry for these models, so we can read from the figure what is the maximum value of the compositeness scale that can be reached. As can be expected the differences with the Standard Model prediction (dotted line) are very large for $\Lambda = 1\ TeV$

and decrease when increasing the value of Λ. In Fig. 7b, where we have plotted the predictions of the AA and LR models for their most sensitive asymmetry, A^{-+}_{RR} the same behavior appears except in the AA model for $\Lambda = 1\ TeV$ for which an accidental cancelation occurs at high Q^2 in such a way that the differences with the Standard Model are better tested at $Q^2 \sim 1 \times 10^4\ GeV^2$. For higher values of Λ, however the cancelation disappears and the signal is again clearer at values of $Q^2 \simeq 2 \times 10^4\ GeV^2$. Finally, in Figs. 7c and d we show the predictions of the VV and LR models for their most sensitive asymmetries: A^{--}_{LR} and A^{-+}_{RR}, respectively. Requiring for the asymmetry measurement the same precission as we did in section 2, we see that one can probe values of Λ up to 5 to 11 TeV, depending on the model. The same values of the compositeness scale can be reached measuring the cross-sections with a precission of $\sim 12\%$. It depends then on the sistematic errors, that one expects to be larger in cross-section measurements than in asymmetry measurements, wether the best quantities to look for contact term effects are the asymmetries or the cross-sections themselves.

3. Summary.

We have studied the modifications to the neutral current cross sections and asymmetries produced by the presence of a new, heavy Z_2 and a possible eq contact term at HERA. For definiteness, we have concentrated on four particular models in the first case. Three of them are based in an E_6 GUT and the forth is a left-right symmetric model. In all the cases the effects on the cross-sections are small, even for a rather light Z_2 and at the highest Q^2 values of attainable at HERA. If polarized beams are available, however, the study of the charge, polarization and mixed asymmetries allows to probe higher values of m_{Z_2}. Assuming a precission in the asymmetry measurements of $\delta A = 0.04$ (0.08) and choosing in each case the most sensitive asymmetry, one will be able to detect the effects of a second Z up to the following masses (taking the case $\theta = 0$)

- Model A 300 (200) GeV
- Model B 250 (150) GeV
- Model C 150 GeV (no interesting bound)
- LR model 650 (400) GeV.

Moreover, if a Z' exists in this mass range, the comparison of its effects on the different asymmetries will allow to determine some of its couplings and to separate it from from other possible sources of modifications to the Standard Model asymmetries.

If leptons and quarks are composite objects, on the other hand, one expects that their interactions should differ from the Standard Model predictions at high enough energies. These modifications are normally parametrized in terms of four-fermion contact interactions. We have also studied six different contact terms of the current-current type. In this case both, cross-sections and asymmetries, show clear deviations from the Standard model predictions

for values of Λ not already excluded by present experimental bounds. Cross-sections, however, are expected to have larger systematic errors than asymmetries. Requiring the same precission for asymmetry measurements as we did before the maximum values of Λ that can be probed are

$$\Lambda \simeq 5 - 10\,(4-7)\,TeV, \tag{34}$$

depending on the model. The higher values of Λ correspond to the RL model, using the A_{LR}^{++} asymmetry, while the lower values of Λ are for the LL model using A_{LR}^{--}. Again, the use of polarized electron beams allow to study the chiral structure of the contact term at the same time that improves the maximum value of Λ that can be reached.

I want to thank R. Rückl for many useful discussions on the subjects covered in this lectures.

Figure Captions

1. Asymmetries for $m_{Z_2} = 200\ GeV$ and $\theta = 0$ as a function of $\cos\alpha$. The dotted line represents the Standard Model value.

2. Diagrams contributing to the corrections to V_{ud} [12].

3. (a) Contours in the plane (m_{Z_2}, θ) for which $\delta A = 0.04$ in model A for A_{LR}^{--} (solid line), A_{RR}^{-+} (dash-dotted line) and A_{RL}^{-+} (dashed line). The thick line is the present experimental bound from ref. [13] and the dotted line is the extrapolation following the rule $\theta \sim 1/m_{Z_2}$.

   (b) The same as Fig. 3a for model B and A_{LR}^{--} (solid line), A_{RR}^{-+} (dash-dotted line) and A_{LR}^{-+} (dashed line).

   (c) The same as Fig. 3a for model C.

4. Polarization asymmetry in $e^+e^- \to \mu^+\mu^-$ as a function of the center of mass energy for models A (dashed line), B (dash dotted line) and C (dotted line). We have taken $m_{Z_2} = 250\ GeV$ and $\Gamma_{Z_2} = 27 m_{Z_2}/1000$ with the corresponding branching ratios (see Table 2) assuming $\theta = 0$. The solid line is the standard model prediction.

5. The same as in Fig. 3b for the Left-Right Symmetric Model assuming $x_L = x_R$.

6. Structure functions F (eq.(33)) for e_L^- (a), e_R^- (b), e_L^+ (c) and e_R^+ (d) beams. The predictions of the RL and RR model for e_L^- and e_R^+ beams are the same as the Standard Model prediction (solid line). The same happens for the LR and LL models with e_R^- and e_L^+ beams.

7. (a) Most sensitive asymmetry for the LL (long-dashed line) and the RR (long-dash dotted line) models as a function of Q^2 for various values of Λ at $x = 0.3$. The Standard Model asymmetry is given by the solid line.

   (b) The same as Fig. 7a for the AA (dotted line) and LR (dashed line) models.

   (c) The same as Fig. 7a for the VV model (dash-dotted line).

   (d) The same as Fig. 7a for the RL model (dash double-dotted line).

References

[1] J. Ellis, New Frontiers in Particle Physics, eds. J.W. Cameron et al. (World Scientific, Singapore, 1986), p. 225.

[2] E. Fahri and L. Susskind, Phys. Rep. 74 (1981) 277.
M.E. Peskin, Proc. Int. Symp. on Lepton and Photon Interactions at High Energy, Kyoto 1985, eds. M. Konuma and K. Takahashi (Kyoto Univ., Kyoto 1985) p. 714.

[3] P. Langacker, Phys. Rep. 72 (1981) 185.

[4] W. Buchmüller, These proceedings.

[5] Q. Shafi and Ch. Wetterich, Phys. Lett. 73B (1978) 65.

[6] P. Candelas, G. Horowitz, A. Strominger and E. Witten, Nucl. Phys. B258 (1985) 46.
E. Witten, Nucl. Phys. B258 (1985) 75.
M. Dine, V. Kaplunovsky, M. Mangano, C. Nappi and N. Seiberg, Nucl. Phys. B259 (1985) 549.

[7] F. del Aguila, G. Blair, M. Daniel and G.G. Ross, Nucl. Phys. B272 (1986) 413.

[8] R.N. Mohapatra, Quarks and Leptons and Beyond, eds. H. Fritzsch, R.D. Peccei, H. Saller and F. Wagner, Plenum Press, New York (1985) p. 219.

[9] W.J. Marciano and A. Sirlin, Phys. Rev. D29 (1984) 945.

[10] F. Cornet and R. Rückl, Phys. Lett 184B (1987) 263.

[11] G. Ingelman, these Proceedings;
R. Rückl, Proceedings of the ECFA Workshop on LEP 200, Aachen 1986, eds. A. Böhm and W. Hoogland, CERN 87-08 and ECFA 87/108, p. 453.

[12] W.J. Marciano and A. Sirlin, Phys. Rev. D35 (1987) 1672.

[13] U. Amaldi et al. Phys. Rev. D36 (1987) 1385.

[14] F. del Aguila, G.A. Blair, M. Daniel and G.G. Ross, CERN-TH. 4376/86.

[15] E. Cohen, J. Ellis, K. Enqvist and D.V. Nanopoulos, Phys. Lett. 165B (1985) 76.

[16] L.E. Ibañez and J. Mas, CERN-TH. 4426/86.

[17] M. Dine et al., Nucl. Phys. B259 (1985) 549.

[18] F. Cornet and R. Rückl, DESY preprint (in preparation).

[19] D.W. Duke and J.F. Owens, Phys. Rev. D30 (1984) 49.

[20] V.D. Angelopoulos, J. Ellis, D.V. Nanopoulos and N.D. Tracas, Phys. Lett. 176B (1986) 203.

[21] Paula J. Franzini and Frederick J. Gilman, Phys. Rev. 35D (1987) 855.

[22] J.P. Ader, S. Narison, and J.C. Wallet, Phys. Lett. 176B (1986) 215.

[23] G. Arnison et al. (UA1), Phys. Lett. 126B (1983) 398.
P. Bagnaia et al. (UA2), Phys. Lett. 129B (1983) 130.

[24] F. del Aguila, M. Quirós and F. Zwirner, Nucl. Phys. B287 (1987) 419.

[25] see also ref. [13].

[26] see also M.J. Duncan and P. Langacker, Nucl. Phys. B277 (1986) 285.

[27] see also H.E. Haber, Supercollider Physics, ed. D.E. Soper (World Scientific Pub. Co., Singapore, 1986) p. 194.

[28] V. Barger, N.G. Deshpande, J.L. Rosner and K. Whisnant, University of Wisconsin preprint MAD/PH/299 (1986).
D. London and J.L. Rosner, Phys. Rev. D34 (1986) 1530.

[29] R.N. Mohapatra and G. Senjanović, Phys. Rev. Lett. 44 (1980) 912 and Phys. Rev. 21D (1981) 165.

[30] E.J. Eichten, K.D. Lane and M.E. Peskin, Phys. Rev. Lett. 50 (1983) 811.

[31] R. Rückl, Nucl. Phys. B234 (1984) 91.

[32] F. Cornet and R. Rückl, DESY preprint (in preparation).

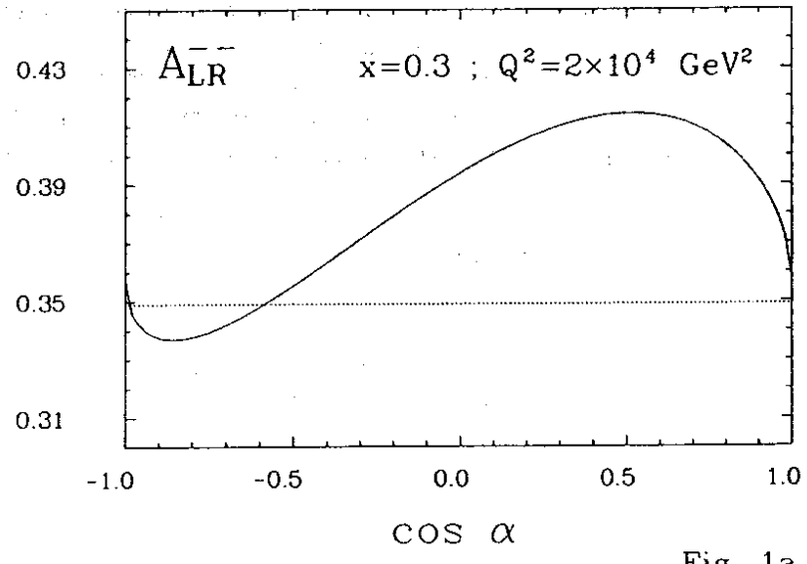

Fig. 1a

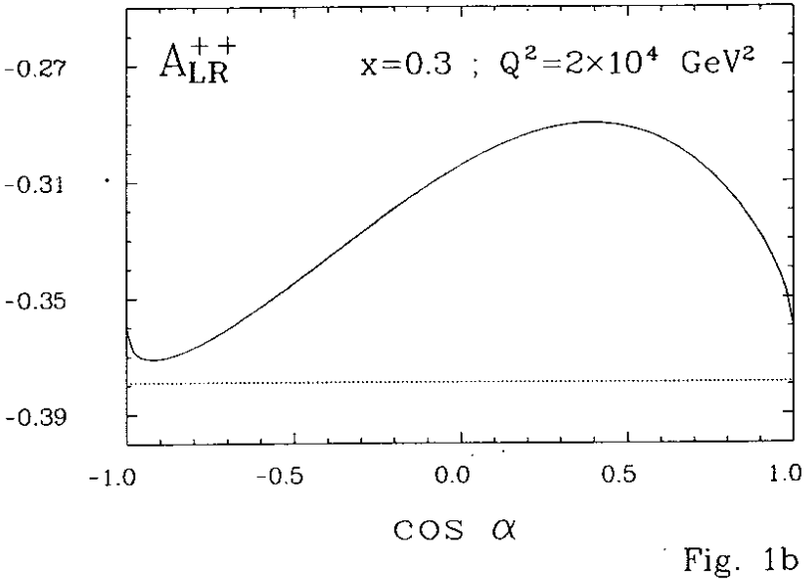

Fig. 1b

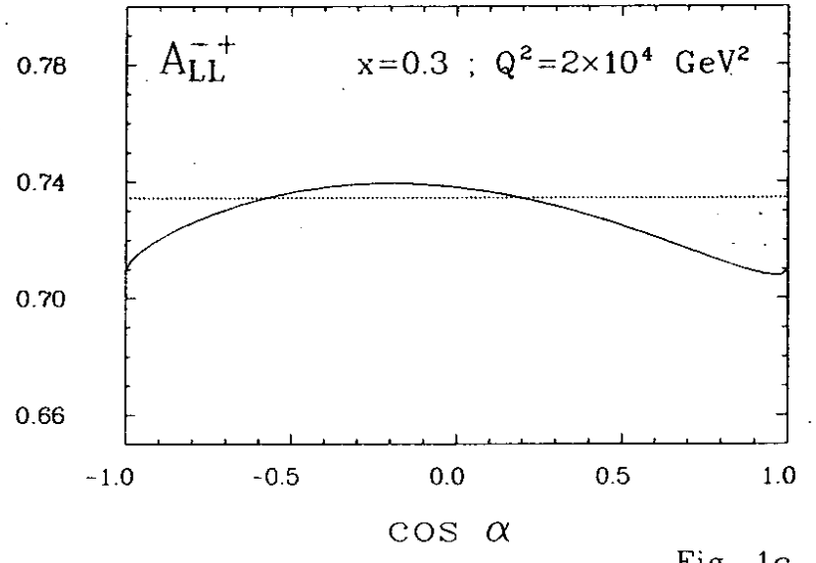

Fig. 1c

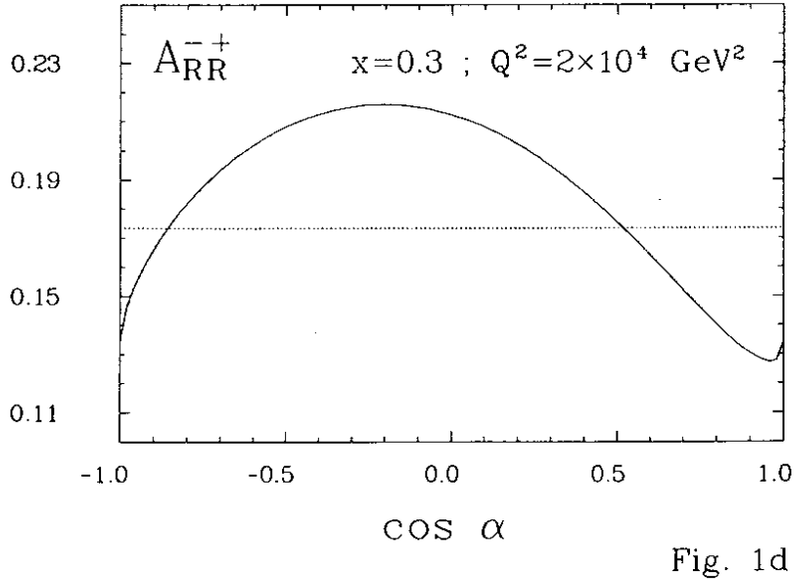

Fig. 1d

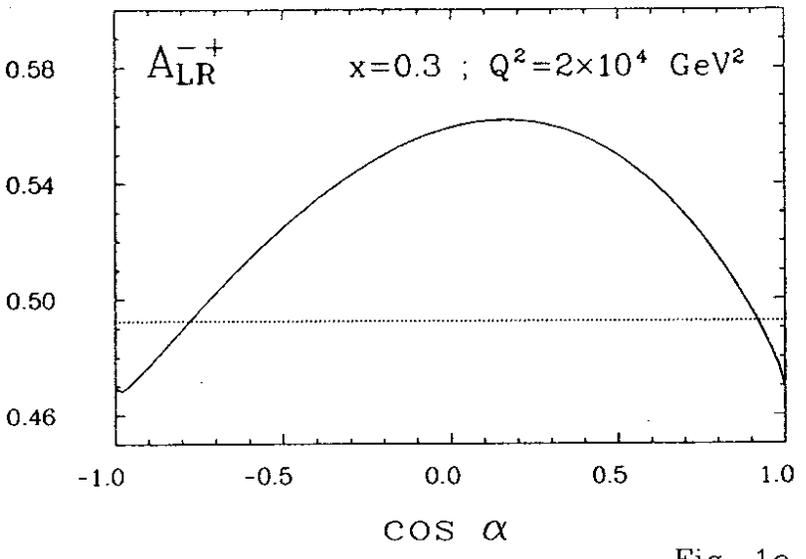

Fig. 1e

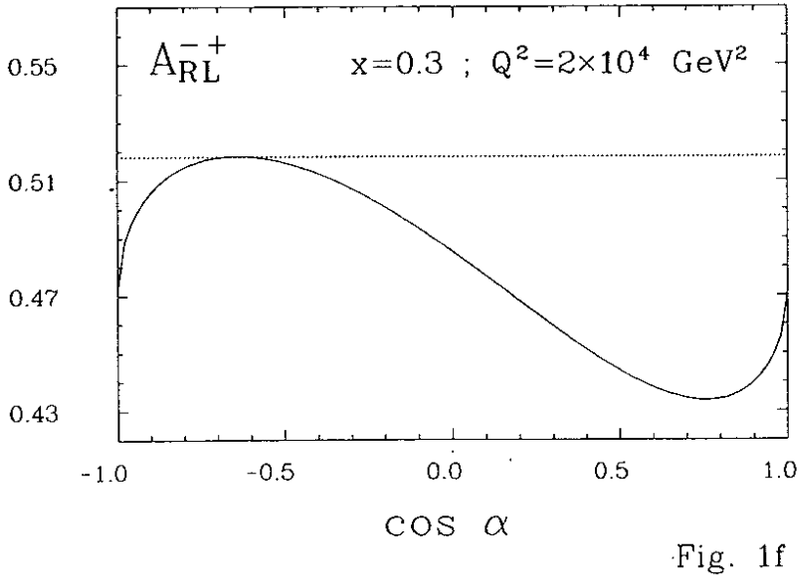

Fig. 1f

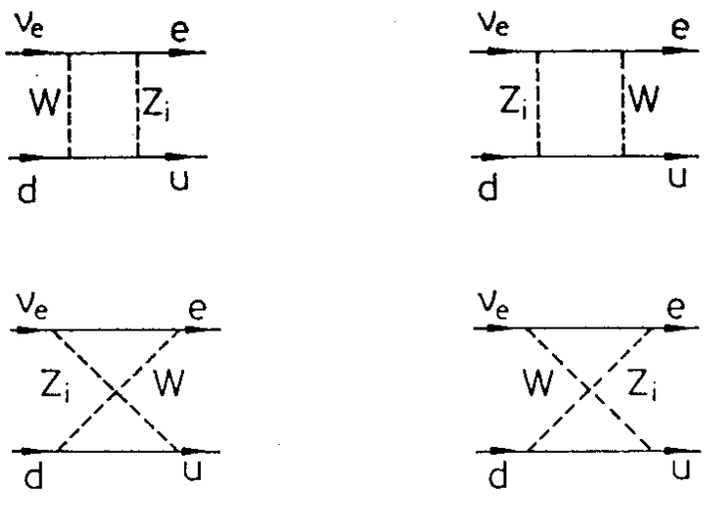

Fig. 2

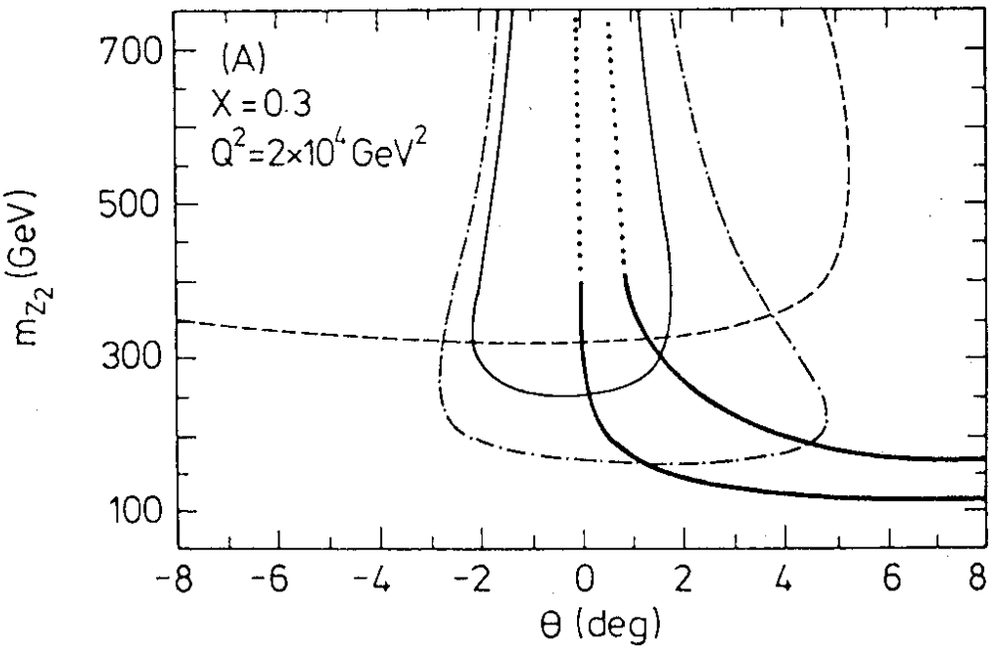
(A)
X = 0.3
$Q^2 = 2\times10^4\ GeV^2$
700
500
300
100
m_{Z_2} (GeV)
-8
-6
-4
-2
0
2
4
6
8
θ (deg)

Fig. 3a

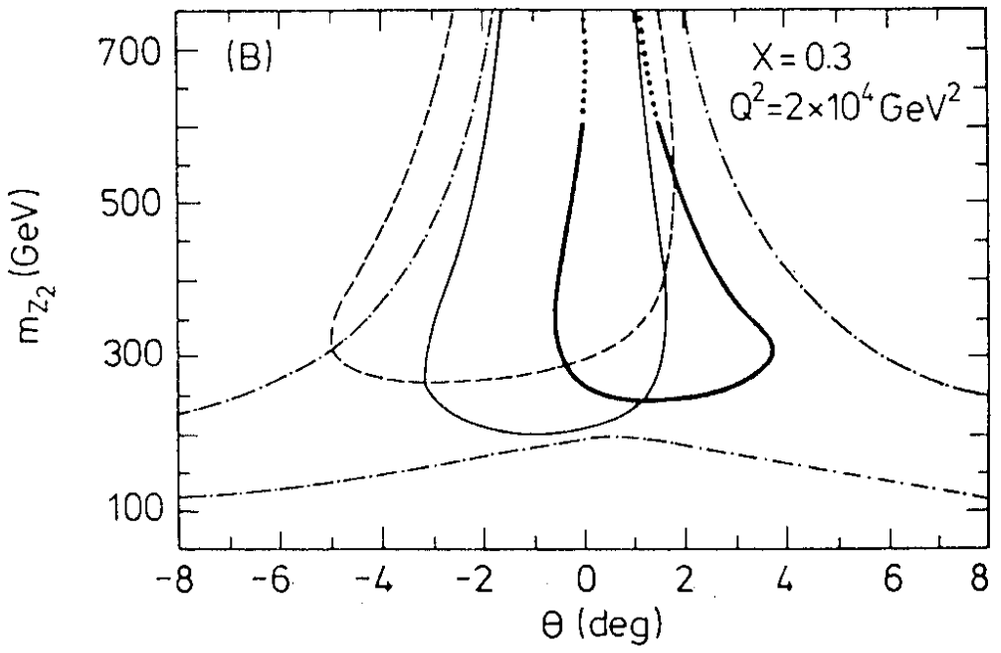
(B)
X = 0.3
$Q^2 = 2\times10^4\ GeV^2$
700
500
300
100
m_{Z_2} (GeV)
-8
-6
-4
-2
0
2
4
6
8
θ (deg)

Fig. 3b

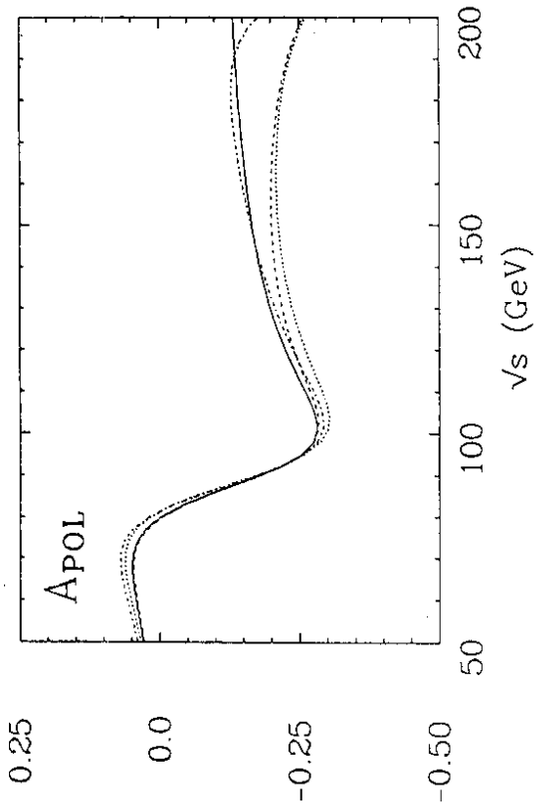
A_{POL}
0.25
0.0
-0.25
-0.50
50
100
150
200
$\sqrt{s}$ (GeV)

Fig. 4

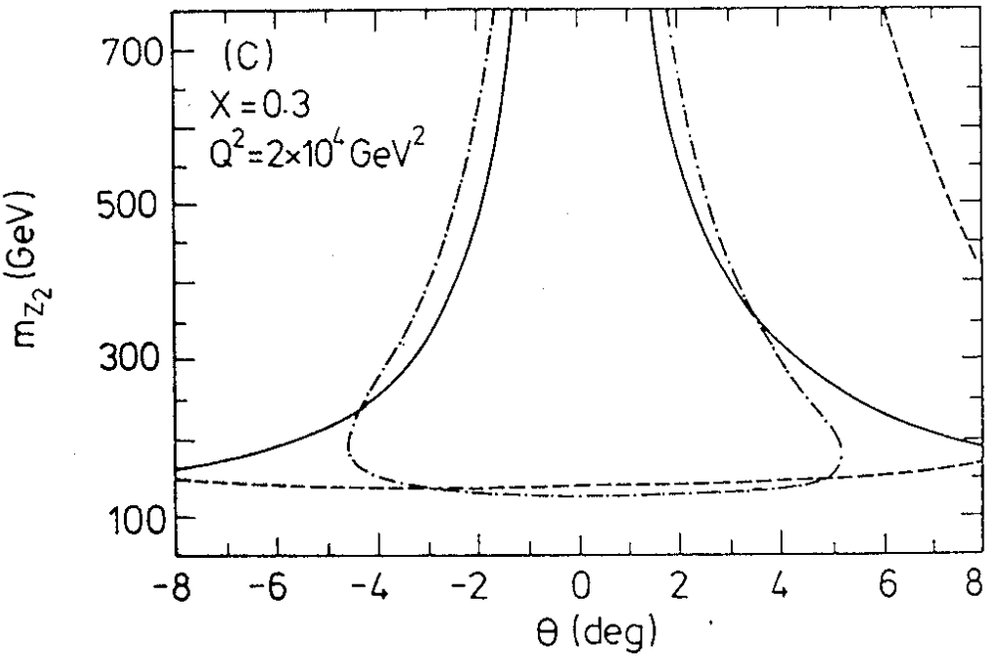
(C)
X = 0.3
$Q^2 = 2 \times 10^4$ GeV^2
m_{Z_2} (GeV)
700
500
300
100
-8
-6
-4
-2
0
2
4
6
8
θ (deg)

Fig. 3c

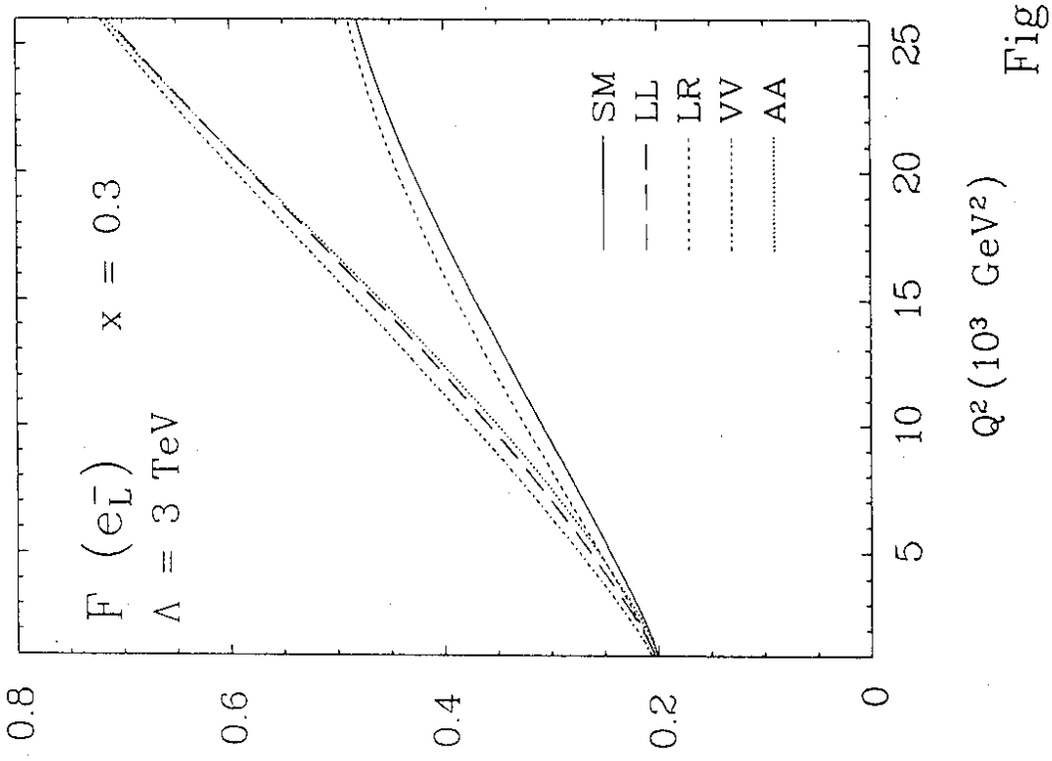
F (e_L^-)
Λ = 3 TeV
x = 0.3
SM
LL
LR
VV
AA
0.8
0.6
0.4
0.2
0
5
10
15
20
25
Q² (10³ GeV²)

Fig. 6a

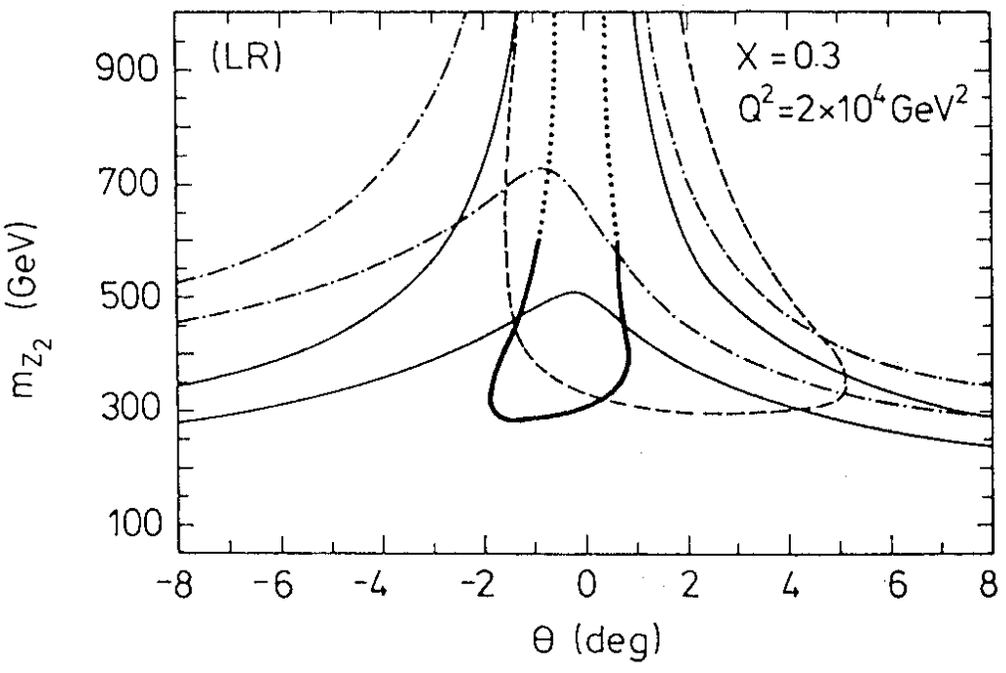
(LR)
X = 0.3
Q²=2×10⁴GeV²
900
700
500
300
100
m_Z2 (GeV)
-8
-6
-4
-2
0
2
4
6
8
θ (deg)

Fig. 5

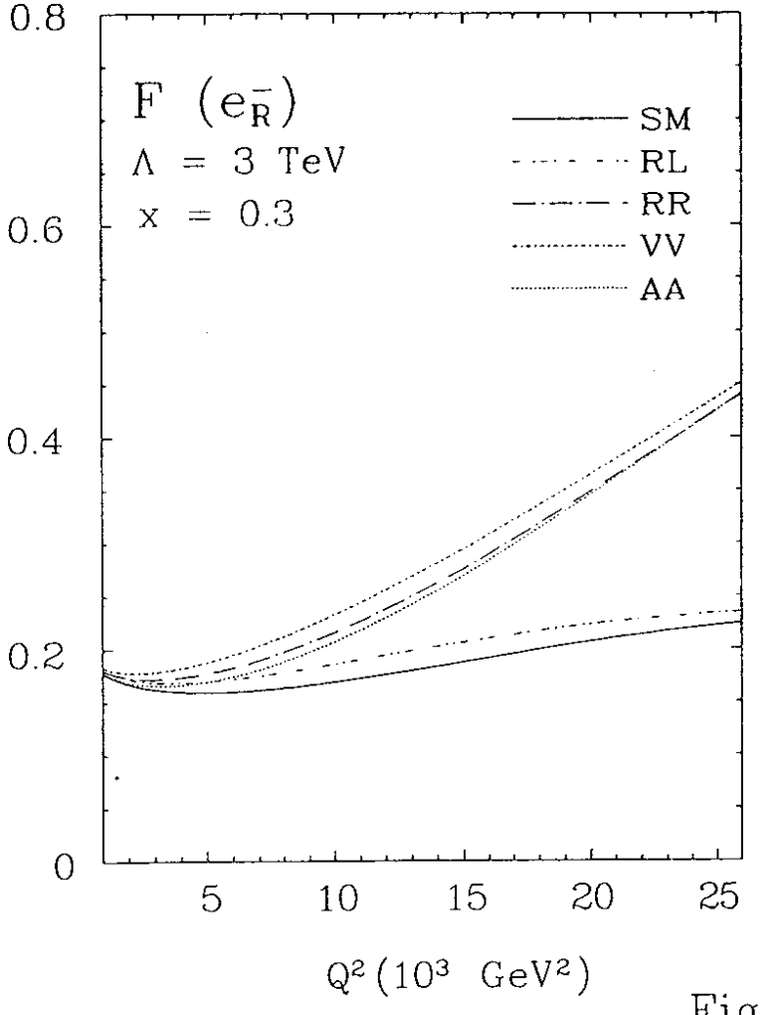
F (e_R^-)
Λ = 3 TeV
x = 0.3
SM
RL
RR
VV
AA
0.8
0.6
0.4
0.2
0
5
10
15
20
25
$Q^2(10^3\ GeV^2)$

Fig. 6b

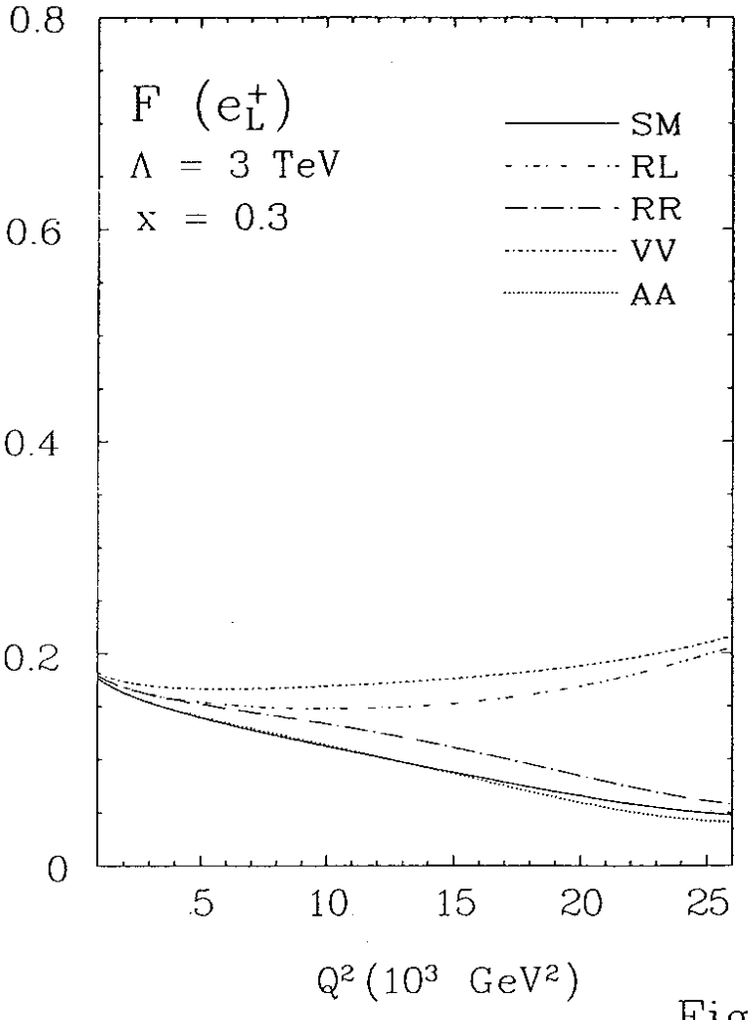
F (e_L^+)
Λ = 3 TeV
x = 0.3
SM
RL
RR
VV
AA
0.8
0.6
0.4
0.2
0
5
10
15
20
25
$Q^2(10^3\ GeV^2)$

Fig. 6c

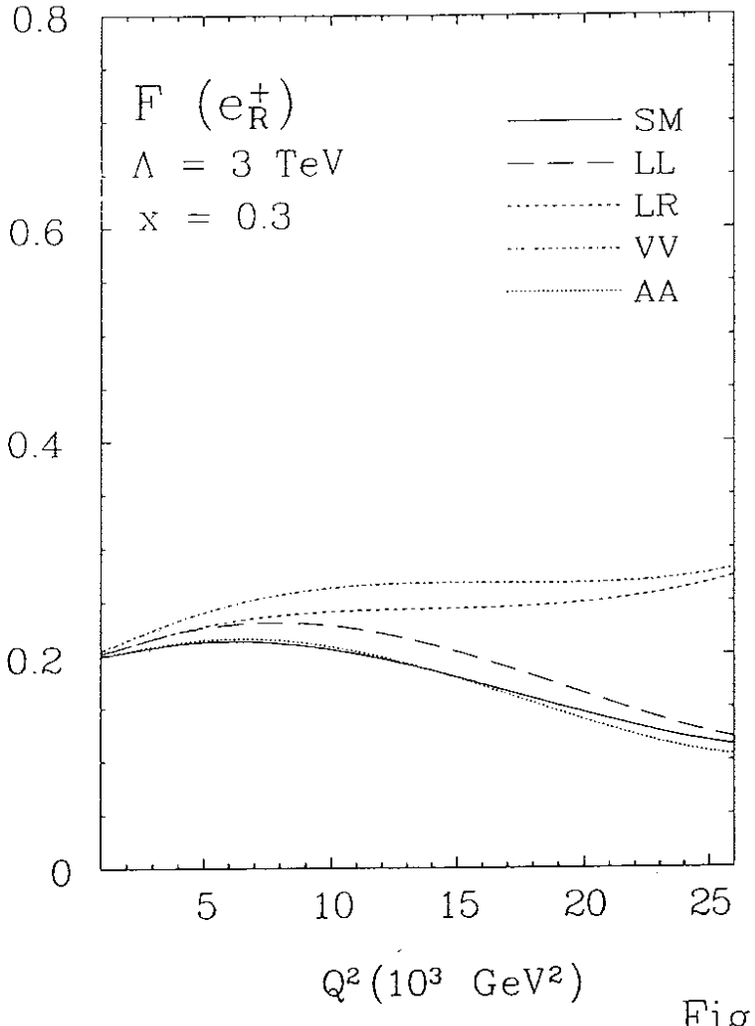
F (e_R^+)
Λ = 3 TeV
x = 0.3
SM
LL
LR
VV
AA
0.8
0.6
0.4
0.2
0
5
10
15
20
25
$Q^2(10^3\ GeV^2)$

Fig. 6d

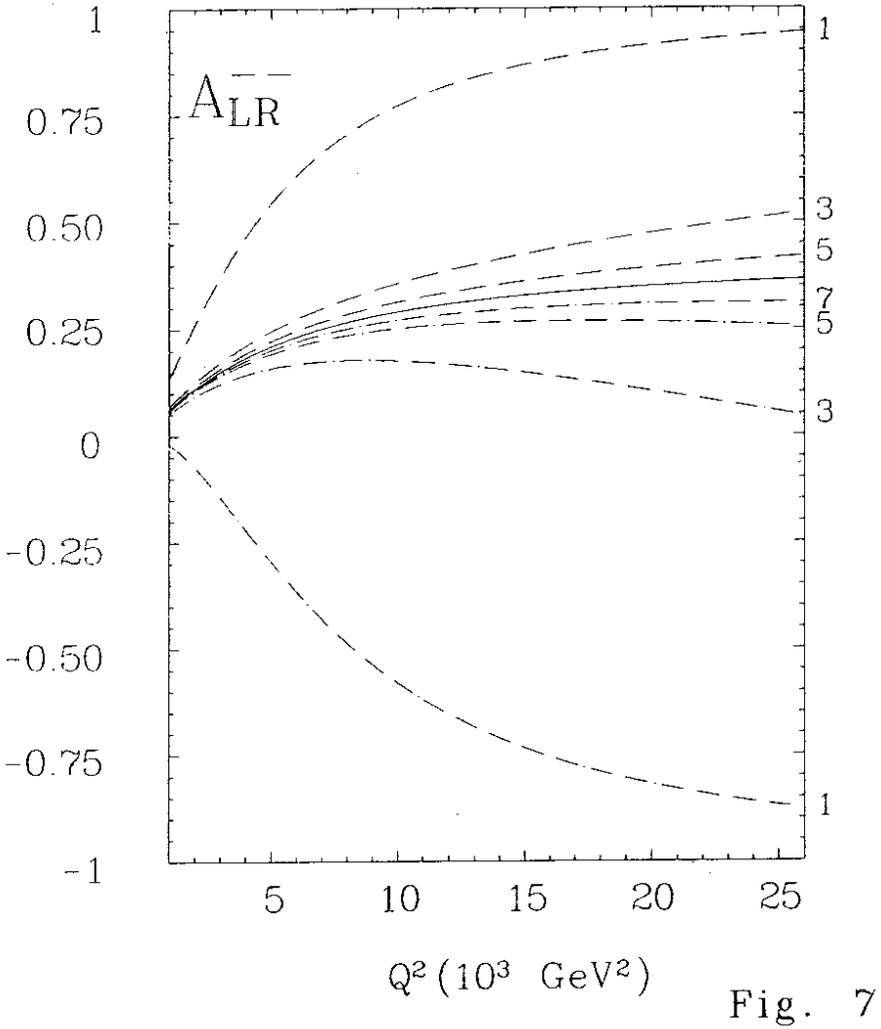
A_{LR}^{--}
1
0.75
0.50
0.25
0
-0.25
-0.50
-0.75
-1
1
3
5
7
5
3
1
5
10
15
20
25
$Q^2(10^3\ GeV^2)$

Fig. 7a

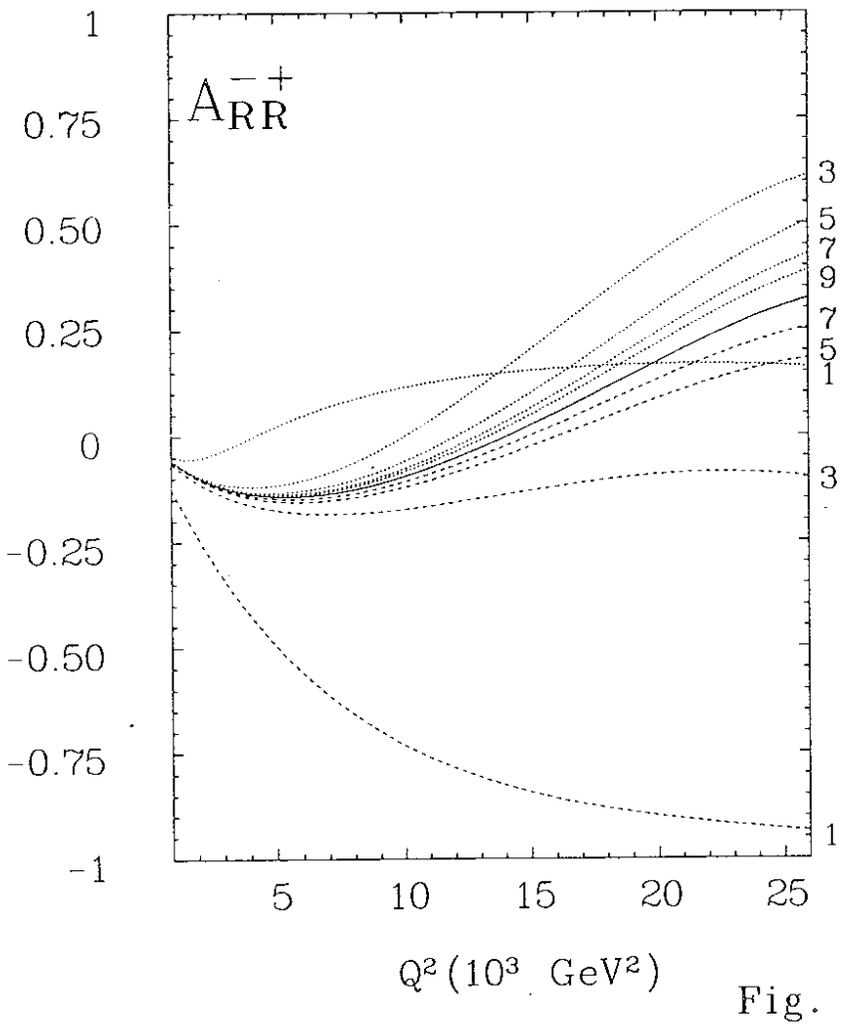
A_{RR}^{-+}
1
0.75
0.50
0.25
0
-0.25
-0.50
-0.75
-1
5
10
15
20
25
$Q^2(10^3\ GeV^2)$
3
5
7
9
7
5
1
3
1

Fig. 7b

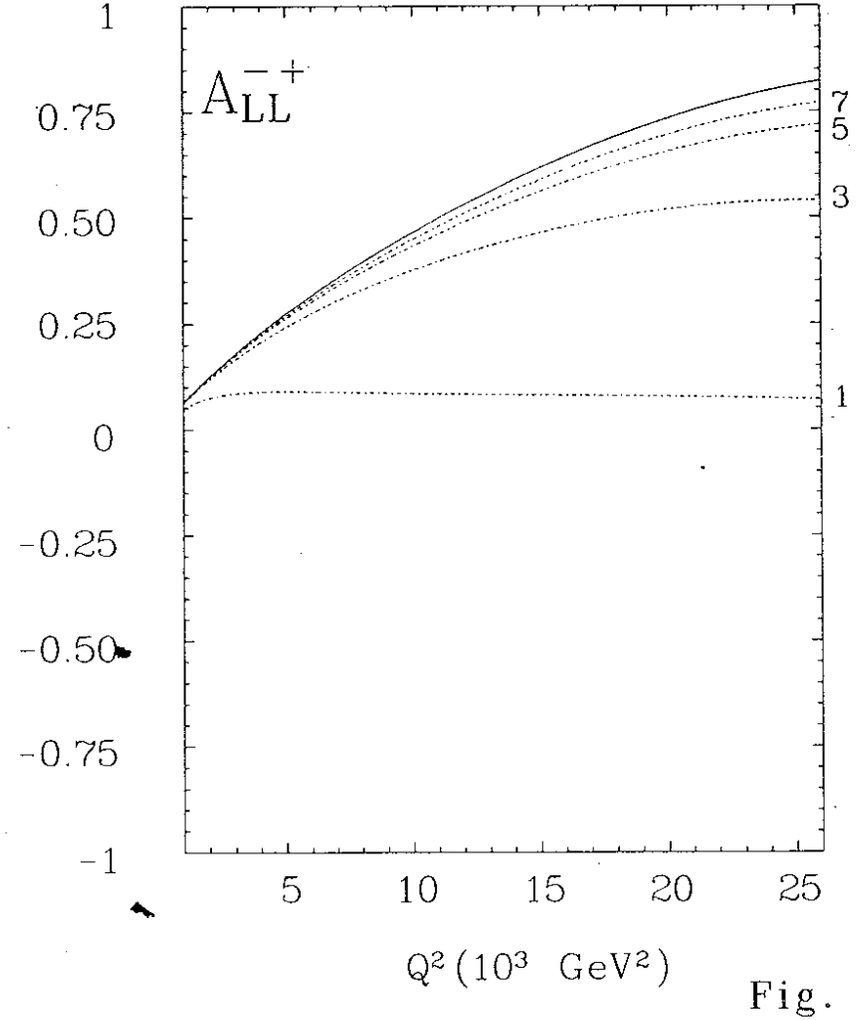
A_{LL}^{-+}
1
0.75
0.50
0.25
0
-0.25
-0.50
-0.75
-1
5
10
15
20
25
$Q^2(10^3\ GeV^2)$
7
5
3
1

Fig. 7c

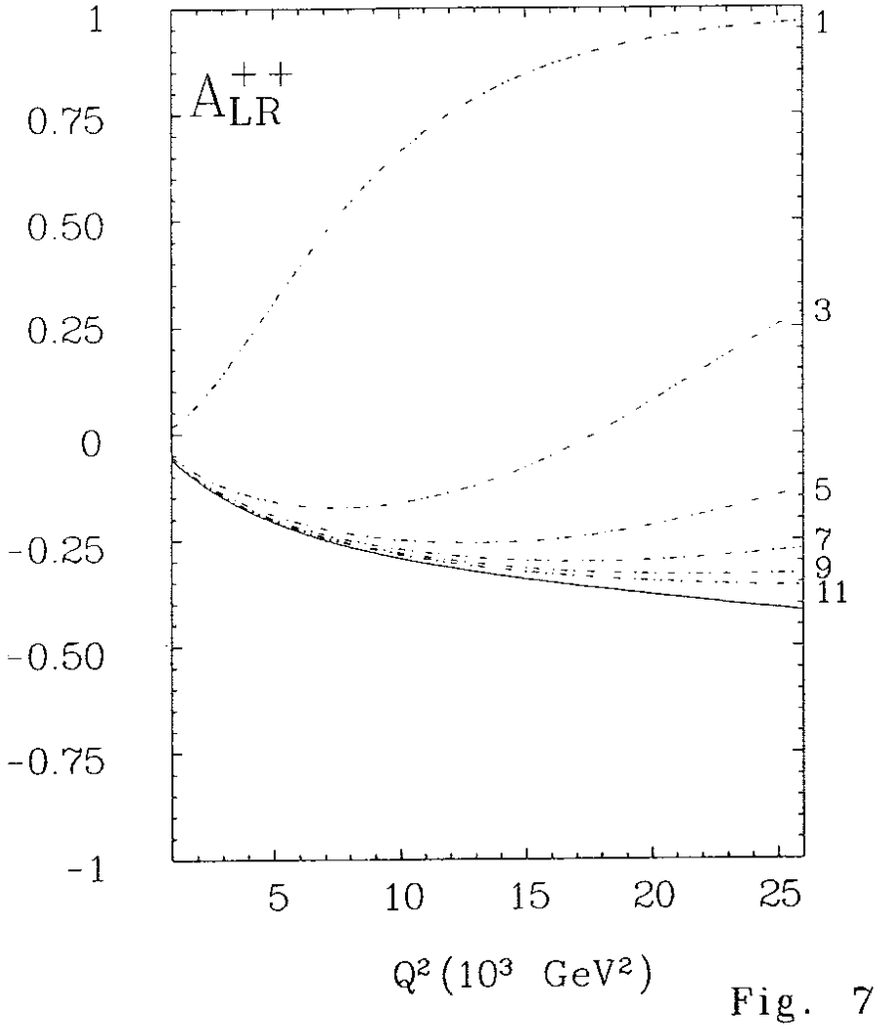

Fig. 7d